A Kinetic and Spectroscopic Study of the CH_3I-Cl and ICH_2I-Cl Adducts†

T. J. Gravestock, M. A. Blitz, and D. E. Heard*

School of Chemistry, University of Leeds, Leeds, LS2 9JT, U.K.

Received: January 15, 2008; Revised Manuscript Received: March 20, 2008

Laser-induced fluorescence from the CH_3I-Cl and ICH_2I-Cl adducts formed in association reactions between chlorine atoms and CH_3I and CH_2I_2 has been observed for the first time. The LIF excitation and dispersed fluorescence spectra have been measured in the range 345−375 nm and 380−480 nm, respectively, at 204 and 296 K. The excitation spectra exhibit vibrational fine structure, and a semiquantitative analysis of the spectra yields a similar binding energy for both adducts of ∼60 kJ mol^{-1}. The adduct fluorescence is efficiently quenched by N_2 and exhibits a zero-pressure lifetime of ∼25 − 30 ns. Using LIF excited from the CH_3I-Cl and ICH_2I-Cl adducts, the kinetics of the reactions of atomic chlorine with methyl iodide and diiodomethane have been investigated, the results showing that both reactions proceed via two independent channels, an association reaction to form the adduct and a bimolecular abstraction reaction. At $T \sim 200$ K, the association reaction is predominant, and CH_3I-Cl formation is irreversible, with rate coefficients for adduct formation found to be pressure-dependent and in reasonable agreement with the literature. At ∼200 K, removal of the adduct is dominated by reaction with radical species (CH_3 and ClSO) and by self-reaction, which proceed at close to the gas kinetic limit. At 296 K, CH_3I-Cl formation is reversible, and the equilibrium constant, $K_p = (70.9 \pm 27.4) \times 10^3$ atm^{-1}, was determined, which is in excellent agreement with the literature, and the adduct does not significantly react with CH_3I. The uncertainty is at the 95% confidence level (2σ) and includes systematic errors. At ∼200 K, the ICH_2I-Cl adduct is again stabilized, with pressure-dependent rate coefficients reaching the high pressure limit at lower pressures than for the $Cl + CH_3I$ reaction. At room temperature, the ICH_2I-Cl adduct is removed via an additional unimolecular decomposition channel, which dominates over the reversible decomposition channel to reform $Cl + CH_2I_2$. Neither adduct was observed to undergo significant reaction with molecular oxygen at ∼200 or 296 K, with an upper limit rate coefficient determined as $k < 10^{-16}$ cm^3 molecule^{-1} s^{-1}.

Introduction

The removal of most organic species emitted into the atmosphere is controlled by reaction with hydroxyl radicals (OH) and/or solar photolysis. Although analogous reactions with chlorine atoms generally have larger rate coefficients,[1–8] there is much uncertainty with respect to the atmospheric concentration of Cl[9,10] and, therefore, its contribution to the oxidizing capacity of the troposphere. Recent observations and inferences of high concentrations of chlorine atom precursors in the marine boundary layer (MBL)[11,12] and the urban troposphere[13,14] suggest that the atmospheric oxidation of trace species may be dominated by reaction with Cl under localized conditions[15] having a significant effect on, for example, local ozone concentrations. Modeling studies[16,17] have found that Cl atoms are an important sink of atmospheric methane (CH_4), an important greenhouse gas, particularly in the free troposphere,[18] and further laboratory studies of the kinetics and mechanisms of Cl atom reactions are required to assess their atmospheric impact.

There is currently much interest regarding iodine chemistry in the MBL, particularly with respect to the fate and products of the IO self-reaction and new particle formation.[19–22] Knowledge of the loss processes of iodine atom (and hence, IO) precursors in the MBL, such as I_2 or alkyliodides, is key in elucidating the mechanisms of these processes. Because alkyliodides possess photolabile C−I bonds, they are rapidly removed from the atmosphere by photolysis. Their lifetimes range from a few minutes (e.g., diiodomethane, CH_2I_2) to a few days (e.g., methyl iodide, CH_3I).[23] If one assumes a Cl atom concentration of 1×10^5 molecules cm^{-3} in the MBL, which is toward the upper end of estimates, the removal of CH_3I by reaction with Cl is approximately equal to that by OH, with a combined reactive loss of ∼10%, as compared with photolysis. Conversely, the rate coefficient for the reaction of 1-C_3H_7I with Cl is sufficiently high that reactive loss may be more important than photolysis for its removal from the atmosphere.[24] Clearly, the atmospheric significance of these reactions depends on their rate coefficients and products under atmospherically relevant conditions. Recently, a number of studies have inferred the formation of association complexes, or adducts, in reactions of Cl atoms with organic species,[25–28] although little is known about the structure or reactivity of these species.

The kinetics of the $Cl + CH_3I$ reaction was first studied by Kambanis et al.[29] for $T = 273-363$ K and $P \sim 2$ mTorr, yielding the Arrhenius relationship $k(T) = (1.33 \pm 0.49) \times 10^{-11}$ exp $[-(690 \pm 120)/T]$ cm^3 molecule^{-1} s^{-1}. A quantitative conversion of Cl to HCl was observed, which suggests that the reaction proceeds exclusively via a hydrogen atom transfer mechanism. A small, temperature-independent, kinetic isotope effect was observed ($k_H/k_D = 1.09 \pm 0.04$) and interpreted as evidence for the reaction proceeding via the formation of a CH_3I-Cl intermediate, which undergoes unimolecular dissociation at low pressure to yield HCl and CH_2I. Subsequently, the enthalpies of adduct formation at 298 K in the reactions of Cl with HI, CH_3I, and CH_3OCH_2I were calculated by Lazarou et al. to be −31.1, −52.4, and −51.3 kJ mol^{-1}, respectively.[30]

† Part of the "Stephen R. Leone Festschrift."

* Corresponding author.

10.1021/jp800372c CCC: $40.75 © 2008 American Chemical Society
Published on Web 06/03/2008

All adducts involve two-center, three-electron interactions originating from charge transfer of electron density from nonbonding orbitals of iodine to bonding orbitals of the I−Cl bond, whose length is around 2.8 Å (∼0.5 Å longer than in ICl), and the R−I-Cl bond angle is close to 80° with little distortion of the CH_3I molecule. Ayhens et al.[31] studied the Cl + CH_3I reaction using resonance fluorescence detection of Cl atoms for $T = 218-694$ K and $P = 5-500$ Torr in N_2. At $363 < T < 694$ K, the reaction was found to be pressure-independent, with $k(T) = 5.44 \times 10^{-11} \exp[-1250/T]$ cm^3 molecule^{-1} s^{-1}, and a significant kinetic isotope effect was observed ($k_H/k_D = 4.3$ and 3.6 at 373 and 419 K, respectively), indicative of the reaction proceeding via a bimolecular H-atom abstraction mechanism. For $263 < T < 309$ K, Cl atom regeneration was observed in a secondary process and was interpreted as evidence for reversible formation of the adduct; for $T < 250$ K, the reaction became pressure-dependent; and at 218 K and 500 Torr, >99.4% of the reactivity was attributed to adduct formation.[31] The reaction mechanism is given by[31] Scheme 1, where k_{bi} is the bimolecular rate coefficient for the

SCHEME 1

$$CH_2I + HCl \xleftarrow{k_{bi}} CH_3I + Cl \underset{k_{-a}}{\overset{k_a}{\rightleftharpoons}} CH_3I\text{-}Cl$$

formation of CH_2I + HCl, k_a is the rate coefficient for adduct formation, and k_{-a} is the rate of adduct decomposition back to reactants, with k_a and k_{-a} being pressure-dependent. The enthalpy and entropy of adduct formation at 298 K were determined as −53.6 and −88 J K^{-1} mol^{-1}, respectively, giving $K_p = 62.7 \times 10^3$ atm^{-1}, and a theoretical investigation of the CH_3I-Cl adduct was largely in agreement with Lazarou et al.[30] Under typical MBL conditions, the rate coefficient for CH_3I + Cl was found to be $\sim 2.5 \times 10^{-11}$ cm^3 molecule^{-1} s^{-1}.[31]

Goliff and Rowland[32] reacted CH_3I with ^{38}Cl (produced by the thermal neutron irradiation of gaseous $CClF_3$), and the products were monitored by gas chromatography. Although the quantification of inorganic products (HCl) could not be determined due to wall and exchange reactions, $CH_3{}^{38}Cl$ was detected with yields ranging from ∼3% at 343 K to ∼10% at 273 K. At 295 K, no change in the $CH_3{}^{38}Cl$ yield was observed with increasing total pressure from 760 to 4000 Torr, the conclusion being that CH_3Cl formation proceeds via either the direct substitution of Cl for I atoms or the intramolecular rearrangement of a short-lived CH_3I-Cl intermediate.[32] In a smog chamber study, Bilde and Wallington [33] monitored the loss of CH_3I in the constant presence of Cl atoms and observed a large kinetic isotope effect at 1 Torr and 295 K ($k_H/k_D = 6$) with $k_H = (9.0 \pm 1.8) \times 10^{-13}$ cm^3 molecule^{-1} s^{-1}. They concluded that because of the absence of any significant CH_3Cl products (<4%) and an indirectly inferred, unity yield of CH_2I, the reaction proceeds exclusively via a bimolecular H-atom abstraction mechanism. At 700 Torr, the rate coefficient increased slightly to $(1.3 \pm 0.4) \times 10^{-12}$ cm^3 molecule^{-1} s^{-1}, with CH_3Cl detected as a minor product, postulated to be formed from both the intramolecular rearrangement of the CH_3I-Cl adduct and reaction of the CH_3I-Cl adduct with CH_3I, with a yield of ≤20% under atmospherically relevant conditions.[33]

Cotter et al.[24] investigated the reaction of Cl atoms with a number of alkyl iodides, including CH_3I, by the fast-flow discharge flow technique coupled to resonance fluorescence detection of Cl atoms. For $T = 298$ K and $P = 1.5 - 12$ Torr (He), a pressure-independent rate coefficient of $k = (1.51 \pm 0.15) \times 10^{-12}$ cm^3 molecule^{-1} s^{-1} was found for Cl + CH_3I, with the reaction postulated to proceed via either direct hydrogen atom abstraction or the formation of a CH_3I-Cl adduct that is either not stabilized or has already reached the high-pressure limit by 1.5 Torr.

Finally, two recent studies by Enami et al.[27,28] reported the direct observation of a number of RI−Cl (R = CH_3, CH_3CH_2, CH_2Cl, CH_2Br, CH_2I, *n*-C_3H_7, *n*-C_4H_9, *cyclo*-C_6H_{11}, C_6H_5, C_6F_5, and *p*-$CH_3C_6H_4$) adducts by cavity ring-down spectroscopy (CRDS). The absorption cross sections of some of the adducts were reported at four wavelengths between 405 and 532 nm. The absorption maxima of CH_3I-Cl and ICH_2I-Cl were found to be at 405 nm, with absorption cross sections of 2.1×10^{-17} and 4.7×10^{-18} cm^2 molecule^{-1}, respectively. By following the temporal profile of the CH_3I-Cl adduct, the reaction kinetics of the CH_3I + Cl reaction were investigated at 250 K for a *P* (N_2) of 25−125 Torr, and reasonable agreement was found with the results of Ayhens et al.[31] On addition of 5−10 Torr O_2, no additional removal of the adduct was observed. Theoretical calculations of the CH_3I-Cl adduct were in accord with the previous studies,[30,31] and the observed absorption was assigned to the red end of the $3^2A' \leftarrow 1^2A'$ and $4^2A' \leftarrow 1^2A'$ electronic transitions originating at 339.32 and 307.06 nm, respectively, and assigned to $\sigma-\sigma^*$ and $\sigma^*-\sigma^*$ transitions in the ICl bond. A further experimental investigation of the CH_3I-Cl adduct by Dookwah-Roberts et al.[34] is given in the accompanying paper, in which the absorption cross section at 315 nm was found to be $(3.5 \pm 1.2) \times 10^{-17}$ cm^2 molecule^{-1}.

Until very recently, there had been no kinetic investigations of the Cl + CH_2I_2 reaction. Stefanopoulos et al.[47] recently studied this reaction at pressures below 3 mTorr in a Knudsen cell and determined the rate coefficient over the range $T = 273-363$ K to be $k(T) = (4.70 \pm 0.65) \times 10^{-11} \exp[-(241 \pm 33)/T]$ cm^3 molecule^{-1} s^{-1}, with a room temperature value of $(2.12 \pm 0.20) \times 10^{-11}$ cm^3 molecule^{-1} s^{-1}. The reactants and stable products were measured using mass spectrometry, and the reaction proceeded via two abstraction pathways yielding the products HCl (55 ± 10%) and ICl. Ab initio calculations determined the binding energy of the CH_2I_2-Cl adduct (Cl−I bond strength) to be 51.9 kJ mol^{-1}.

Bilde et al.[35] have studied the Cl + CH_2ICl reaction by laser flash photolysis coupled with resonance fluorescence detection of Cl atoms and by FTIR detection of reactants and products in a continuous photolysis smog chamber. Over the range $T = 206-432$ K, the rate coefficient was given by $k(T) = 4.4 \times 10^{-11} \exp(195/T)$ cm^3 molecule^{-1} s^{-1}, with $k(298) = 8.5 \times 10^{-11}$ cm^3 molecule^{-1} s^{-1} and (largely) independent of pressure (5−700 Torr N_2/O_2). From a product analysis, it was inferred that the reaction mechanism predominantly involves I-atom abstraction, producing ICl and CH_2Cl with near unity yield. The results were rationalized by the formation of a $CH_2ClI-Cl$ adduct (to explain the high rate coefficient) whose fate, on energetic grounds, is decomposition to ICl + CH_2Cl, rather than back to reactants (or HCl + CHICl). Kambanis et al.[36] studied the reaction over the range $T = 273-363$ K at very low pressure, $P = 0.6 - 1.5$ mTorr (He), and found a temperature-independent $k = (3.13 \pm 0.27) \times 10^{-11}$ cm^3 molecule^{-1} s^{-1}, with ICl observed as a direct reaction product. A theoretical calculation of the $CH_2ClI-Cl$ adduct gave r(I−Cl) = 2.738 Å. ∠(C−I−Cl)= 76.21° and $CH_2ClI-Cl$ bond enthalpy = 54.8 kJ mol^{-1}. The ICl + CH_2Cl reaction pathway is energetically accessible, and dissociation of the $CH_2ClI-Cl$ adduct to ICl + CH_2Cl is favored on entropic grounds. The smaller rate coefficient may be representative of the low pressures employed, and the lack of a

temperature dependence due to a nonthermal distribution of adduct states.[36] This reaction of $CH_2ICl + Cl$ can be represented by reaction scheme 2, where k_{bi}, k_a, and k_{-a} have the same meanings as Reaction Scheme 1 and k_p is the unimolecular rate coefficient for decomposition of the adduct to form the products $CH_2Cl + ICl$. ICl has been detected as a product of the $CH_2I_2 + Cl$ reaction in a molecular beam investigation.[37] However, this is also the case for $CH_3I + Cl$,[38] where ICl formation may have been favored by the high translational energy of the reactants.

SCHEME 2

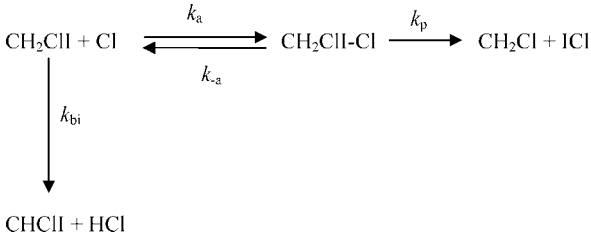

In this paper, we report for the first time the direct detection of the CH_3I-Cl and ICH_2I-Cl adducts using laser-induced fluorescence (LIF) spectroscopy. LIF excitation spectra, dispersed fluorescence spectra, and fluorescence lifetime/quenching measurement of the two adducts are reported, providing information about the internal energy distributions and electronic states of these molecules. We also report, via detection of the adducts, a detailed kinetic study of the $Cl + CH_3I$ and CH_2I_2 reactions at 206 and 296 K. The results provide further insight into the mechanism of Cl + RI reactions.

Experimental Technique

All experiments were performed using a pulsed-laser-photolysis laser-induced fluorescence system (PLP-LIF). The ~500 cm^3 stainless-steel reaction cell consisted of a six-way cross with cylindrical arms surrounded by an insulated reservoir. Temperature measurements were made with a calibrated N-type thermocouple located near the center of the reaction cell. For low temperature experiments close to 200 K, the reservoir was filled with a dry ice/propan-2-ol slurry. The two horizontal cell axes were used as the principal laser axes, fluorescence was detected at the top port of the vertical cell axis by a photomultiplier (PMT), and the cell was evacuated by a rotary vacuum pump. All optical ports were sealed with 50-mm-diameter silica windows, and reagent mixtures were prepared on a gas-handling line consisting of stainless steel tubing linked together by a series of two-way taps and connected to an oil diffusion pump and a rotary-vane pump with a base pressure of $<10^{-5}$ Torr. CH_3I and CH_2I_2 (both Aldrich, 99%) were purified via several freeze−pump−thaw cycles at 77 K prior to their dilution and storage in blackened 10 L glass bulbs. Nitrogen (Air Products, premier grade) and He (BOC, CP grade) were administered directly from their gas cylinders without purification. Gas mixtures were introduced to the reaction cell via the gas handling line and calibrated mass flow controllers, and all concentrations were evaluated from the mass flow rates, dilution factors and reaction cell pressure and temperature, which were measured with a 0−1000 Torr capacitance manometer and an N-type thermocouple, respectively. The reaction cell pressure was adjusted by a combination of the total gas flow rate and throttling of the vacuum pumping system with a suitable valve. For all experiments, chlorine atoms were generated via the 248 nm (KrF excimer laser, Lambda Physik, LPX205) photolysis of thionyl chloride (Cl_2SO, Aldrich 99+ %, purified by several freeze−pump−thaw cycles at 77 K). The photolysis laser energy was measured with an energy meter (Molectron Jmax) at the rear reaction cell window and could be varied from 2 to 60 mJ $pulse^{-1}$ via a combination of adjusting the operating voltage of the excimer laser and attenuating the photolysis radiation with a series of fine-mesh metal gauzes. At 248 nm, the major photolysis channel of thionyl chloride yields Cl atoms and ClSO radicals (96.5%), although a minor channel also produces SO radicals and molecular chlorine.[26] Because the photolysis wavelength is near the absorption maxima of CH_3I ($\sigma_{(248.4\ nm)} = 8.64 \times 10^{-19}$ cm^2 $molecule^{-1}$)[28] and CH_2I_2 ($\sigma_{(248.4\ nm)} = 1.57 \times 10^{-18}$ cm^2 $molecule^{-1}$),[28] a low photolysis energy of ~2 mJ $pulse^{-1}$ was employed for kinetic experiments, ensuring minimum generation of radical species from the photolysis of methyl iodide (<0.5% photolyzed) and diiodomethane (<1% photolyzed). The concentration of radicals generated from CH_3I or CH_2I_2 can be obtained from these percentages, and the CH_3I and CH_2I_2 concentrations are given in Tables 1 and 4. For spectroscopic experiments, where the chemistry occurring is of less significance, the photolysis energy was typically 50 mJ $pulse^{-1}$.

Tuneable probe radiation with ~3 mJ $pulse^{-1}$ in the range 345−375 nm was generated by a dye laser (Lambda Physik, FL3002), operating on a DMQ dye, which was pumped by a XeCl excimer laser (Lambda Physik, LPX105) at 308 nm. The photolysis and probe laser beams were directed orthogonally through the reaction cell using suitable laser mirrors and intersected at the center of the cell. An iris situated at the front cell window was used to give a photolysis laser beam with circular profile of ~7 mm diameter. All the kinetic data determined in this work were found to be independent of laser pulsed repetition frequency (PRF), with kinetic and spectroscopic experiments performed at PRFs of 5 and 10 Hz, respectively. Adduct fluorescence was partially discriminated from the exciting laser radiation by means of a Perspex filter. The analogue signal from the PMT was sent to an oscilloscope and a gated integrator and boxcar averager before being digitized and stored on a personal computer. Fluorescence lifetimes were measured by recording the temporal profile of adduct fluorescence (and the excitation laser pulse) on a digital oscilloscope. The photolysis and probe lasers were triggered by a delay generator (SRS DG535) operating under computer control, allowing the time interval between photolysis and probe lasers, Δt, to be varied to obtain the temporal evolution of the adduct concentration. The oscilloscope and boxcar averager were also triggered by the delay generator at the same time as the probe laser. LIF excitation spectra were recorded by monitoring the total fluorescence signal as the wavelength of the dye laser was scanned at constant speed and for a fixed interlaser delay, Δt. Dispersed fluorescence spectra were recorded via the incorporation of a monochromator (Applied Photophysics, *f*/3.4) to the apparatus. Adduct fluorescence, induced by a specific excitation wavelength and Δt, was dispersed by scanning the diffraction grating of the monochromator prior to its detection by the PMT. Additional details are given in the Results sections. The probe laser power was monitored using a photodiode so that the LIF signal could be normalized for changes in laser power.

Results and Discussion

Observation of Laser-Induced Fluorescence from the CH_3I-Cl and CH_2I_2-Cl Adducts. Adduct fluorescence was first detected in an experiment arranged for the LIF detection

TABLE 1: Kinetic Data Obtained in This Work and Other Selected Studies of the $CH_3I + Cl$ Reaction for $T \leq 250$ K[a]

T	P	precursors, M	λ_p	$[Cl_0]$	$[CH_3I]$	k_1	ref
200.0	10.2	CH_3I/Cl_2SO, N_2	248	0.11	113	5.59 ± 1.20	[b]
200.4	40.0			0.13	154	10.5 ± 1.6	[b]
201.9	71.3			0.12	160	15.4 ± 1.2	[b]
203.8	100.2			0.13	168	18.3 ± 1.7	[b]
203.8	100.0			0.12	181	19.3 ± 1.9	[b]
216.2	251.0			0.12	189	28.8 ± 2.3	[b]
215.9	497.4			0.24	371	35.1 ± 3.5	[b]
218	5.1	CH_3I/Cl_2, N_2	355	0.11	1140	3.31 ± 0.52	31
218	10			0.11	982	5.04 ± 0.26	31
218	30			0.10	1160	10.2 ± 0.7	31
218	100			0.14	983	19.8 ± 1.9	31
218	250			0.16−0.33	722	25.0 ± 1.3	31
218	500			0.36	662	29.7 ± 2.6	31
250	10			0.19	990	3.25 ± 0.21	31
250	100			0.10	830	14.3 ± 0.7	31
250	500			0.30	356	24.5 ± 1.9	31
250	25			1−10	9000	4.0 ± 1.0	27
250	125			1−10	9000	20.0 ± 3.0	27

[a] The provided experimental conditions include: T (K), P (Torr), nature of the chlorine atom precursor and bath gas, photolysis wavelength (nm), estimated initial Cl atom concentration and range of CH_3I concentrations employed (10^{12} molecules cm^{-3}), and bimolecular rate coefficients k_1 (10^{-12} cm^3 $molecule^{-1}$ s^{-1}). Note that this study and that of Enami et al.[27] employed spectroscopic detection of the CH_3I-Cl adduct, and Ayhens et al.[31] employed resonance fluorescence detection of Cl atoms. [b] This work.

TABLE 2: Reactions and Rate Coefficients Employed in the FACSIMILE Model Used in This Work[a]

reaction	rate coefficient	ref
(1a) $Cl + CH_3I \rightarrow CH_3I-Cl$	1.88×10^{-11} cm^3 $molecule^{-1}$ s^{-1}	
(1b) $Cl + CH_3I \rightarrow HCl + CH_2I$	1.1×10^{-13} cm^3 $molecule^{-1}$ s^{-1}	31
(2) $Cl \rightarrow$ loss	220 s^{-1}	
(3) $CH_3I-Cl + CH_3I-Cl \rightarrow$ products	3.5×10^{-10} cm^3 $molecule^{-1}$ s^{-1}	34
(4) $CH_3I-Cl + CH_3 \rightarrow$ products	3.0×10^{-10} cm^3 $molecule^{-1}$ s^{-1}	
(5) $CH_3 + CH_3 \rightarrow$ products	5.0×10^{-11} cm^3 $molecule^{-1}$ s^{-1}	42
(6) $CH_3I-Cl + ClSO \rightarrow$ products	k_6	
(7) $CH_3I-Cl \rightarrow$ loss	20 s^{-1}	
(8) $CH_2I_2 + Cl \rightarrow ICH_2I-Cl$	6.7×10^{-11} cm^3 $molecule^{-1}$ s^{-1}	
(−9a) $ICH_2I-Cl \rightarrow CH_2I_2 + Cl$	13 200 s^{-1}	
(9p) $ICH_2I-Cl \rightarrow$ products	13 200 s^{-1}	

[a] All rate coefficients are assigned the appropriate values obtained from this work unless otherwise referenced. Note that reactions (8) and (9) correspond to a modelling exercise concerning the $CH_2I_2 + Cl$ reaction, which is discussed in the text.

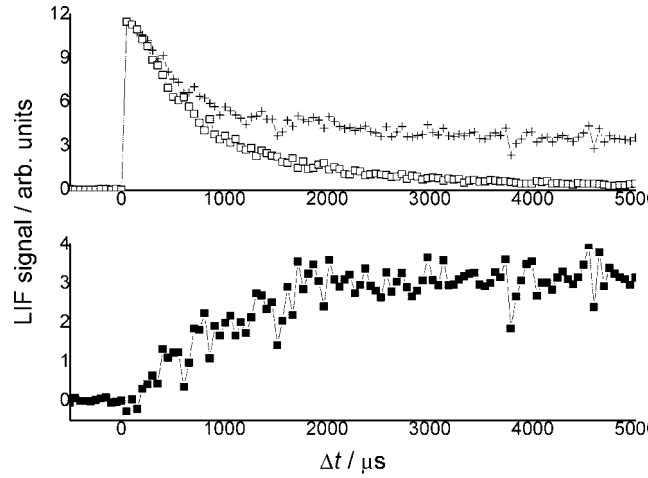

Figure 1. Kinetic traces recorded in a $Cl_2SO/CH_3I/O_2/N_2/248$ nm reaction mixture. The top panel displays traces obtained for excitation wavelengths of 353.16 nm (+) and 355.00 nm (□). The bottom panel displays the CH_2O kinetic trace resulting from their residual. Experimental conditions: $P = 100$ Torr; $T = 296$ K; $[Cl_2SO] = 2.23 \times 10^{13}$ molecules cm^{-3}; $[CH_3I] = 8.8 \times 10^{14}$ molecules cm^{-3}; $[O_2] = 2.43 \times 10^{16}$ molecules cm^{-3}; $[N_2]$ = balance; photolysis laser fluence $F_{(248nm)} = 6.0 \times 10^{16}$ photons cm^{-2}; PRF = 0.5 Hz; excitation laser energy (P_{ex}) = 2.6 mJ $pulse^{-1}$.

of formaldehyde, CH_2O, when Cl atoms were reacted with CH_3I in the presence of O_2. Extremely intense fluorescence, induced by 353.16 nm excitation radiation, was observed at early reaction times, which decayed to a nonzero baseline at larger values of Δt, as shown in Figure 1. Although the presence of CH_2O has been observed (its formation initiated by the reaction of $CH_2I + O_2$),[39] the temporal profile of the fluorescing species was not compatible with formaldehyde, nor was its fluorescence lifetime. Fluorescence from this unknown species was independent of the presence of O_2 and was observed to form with the correct kinetics for a product of the reaction $Cl + CH_3I \rightarrow$ products (see Figures 2,4 and 5 for examples of growth kinetics corresponding to adduct formation). When the excitation wavelength of the probe laser was altered to 355.00 nm (a wavelength where CH_2O absorbs weakly in comparison to 353.16 nm), the intense fluorescence was still observed, although the PMT signal returned to close to the pre-excimer laser background at longer reaction times, as shown in Figure 1. In addition, LIF from the adduct was observed over the entire useful wavelength range of the probe laser dye (~345−375 nm), and these observations suggest that the fluorescence originates from a product of the $CH_3I + Cl$ reaction and, as a result of its relatively broad and unstructured nature, a polyatomic species, consistent with the recent observation of CH_3I-Cl by CRDS.[27]

Upon exchanging CH_3I for CH_2I_2 in the reagent system, a similar fluorescence signal was observed, although with a weaker intensity, presumably originating from the ICH_2I-Cl adduct. We estimate detection limits for CH_3I-Cl and ICH_2I-Cl of $(3.7 \pm 2.0) \times 10^9$ and $(4.7 \pm 3.3) \times 10^{10}$ molecules cm^{-3}, respectively, for a signal-to-noise ratio (S/N) of 1 and an average of 15 laser shots (3 s at a laser PRF of 5 Hz). The fluorescence collection arrangement was relatively crude, and fluorescence from the adducts was not completely discriminated from scattered laser radiation by the Perspex optical filter. It is

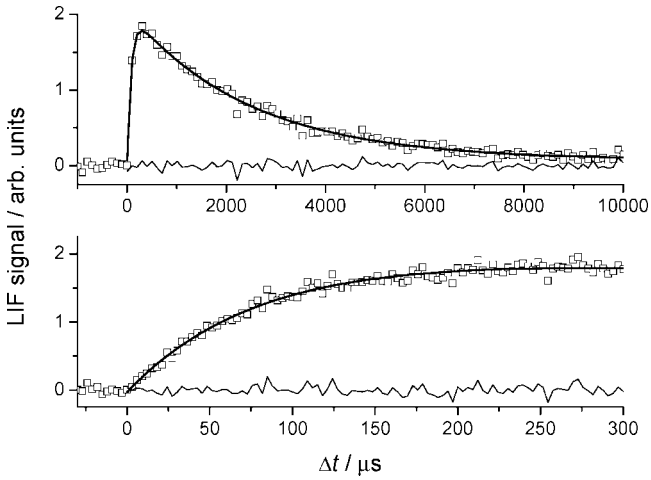

Figure 2. LIF traces of CH_3I-Cl in $Cl_2SO/CH_3I/N_2$/248 nm photolysis mixtures. Both traces were recorded under identical experimental conditions, with the exception of the temporal range. Fits of eq I (—) to the experimental data (□), together with residuals (—) shown by the fainter solid lines. Experimental conditions: $T = 215.9$ K; $P = 494.0$ Torr; $[Cl_2SO] = 1.43 \times 10^{13}$ molecules cm^{-3}; $[CH_3I] = 3.71 \times 10^{14}$ molecules cm^{-3}; $[N_2]$ = balance; PRF = 5 Hz; $F_{(248nm)} = 2.4 \times 10^{15}$ photons cm^{-2}; $\lambda_{ex} = 360.57$ nm.

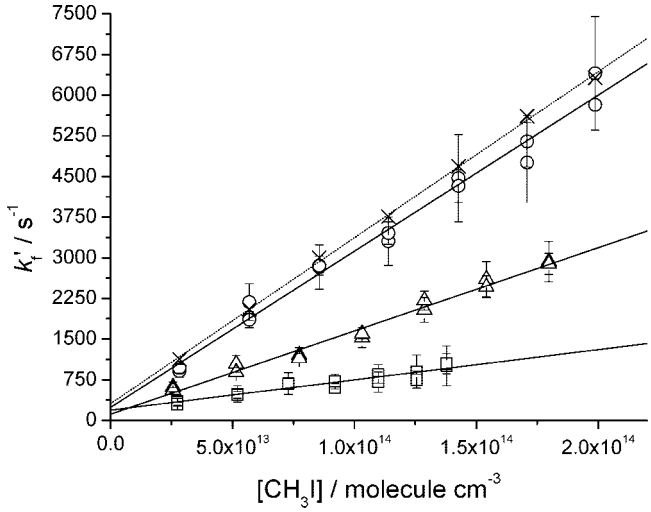

Figure 3. Bimolecular plots for the reaction $CH_3I + Cl$ at $T \sim 200$ K. $T = 200$ K, $P = 10.2$ Torr (□); $T = 202$ K, $P = 71.3$ Torr (Δ); $T = 216$ K, $P = 251.0$ Torr (O). Note that pseudo-first-order formation rates from both small and large Δt ranges are included in the bimolecular analyses. Model simulations of the 251 Torr experiment as discussed in the text (×). Linear fits to the experimental data (—), linear fit to the model simulations (▪▪▪). All bimolecular rate coefficients are listed in Table 1, along with additional experimental conditions. The error bars are 2σ standard uncertainty of the exponential fits to the experimental data.

estimated that, if desired, the detection limit for both species could easily be improved by 2 orders of magnitude using more sophisticated optics and a more discriminative interference filter.

Reaction Kinetics of the Adduct Formed in the Cl + CH_3I Reaction. To confirm the detection of CH_3I-Cl, the reaction kinetics of the $CH_3I + Cl$ reaction were studied at ~200 K and at room temperature by following the temporal evolution of the fluorescing species by LIF in $Cl_2SO/CH_3I/N_2$/248 nm photolysis mixtures. Figure 2 shows some kinetic traces of the fluorescence recorded at 216 K and 494 Torr N_2. Kinetic traces were recorded for both small and large ranges of Δt to accurately determine the adduct growth and decay rates, which were observed on very different timescales under the experimental conditions. For

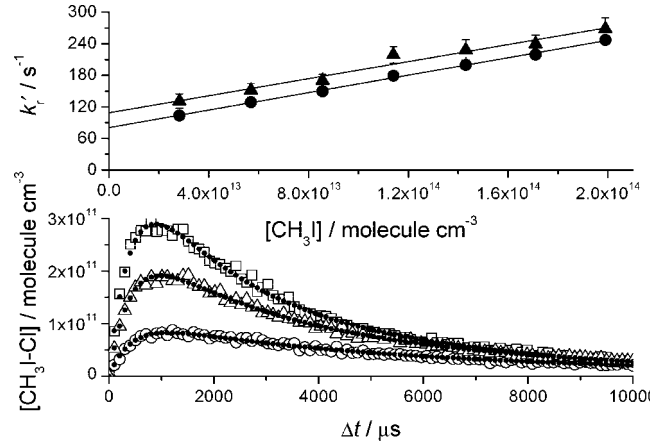

Figure 4. Top panel: CH_3I-Cl removal rate k_r' as a function of $[CH_3I]$ at 216 K and 251 Torr N_2 (experimental data, ▲; modelled data, ●). Bottom panel: kinetic traces of CH_3I-Cl recorded at three different $[Cl_2SO]$; experimental conditions: $T = 204$ K; $P = 100$ Torr; $[CH_3I] = 1.17 \times 10^{14}$ molecules cm^{-3}; $[Cl_2SO]$ (molecules cm^{-3}) = 7.04×10^{12} (O), 1.76×10^{13} (Δ) and 2.81×10^{13} (□); $[N_2]$ = balance; PRF = 5 Hz; $F_{(248nm)} = 2.40 \times 10^{15}$ photons cm^{-2}; $\lambda_{ex} = 360.57$ nm. The scattered points represent the experimental data, and (•••) represent the model fit to the data, which also provides the absolute concentration (see text for details).

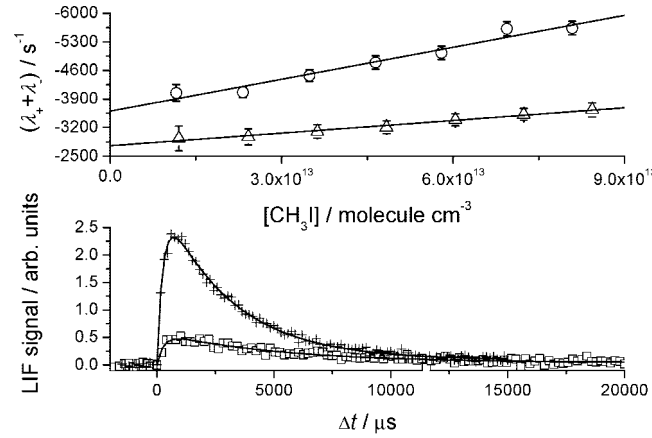

Figure 5. Bottom panel: Fits of eq III to two 296 K kinetic traces of CH_3I-Cl recorded in a $Cl_2SO/CH_3I/N_2$/248 nm photolysis mixture. Experimental conditions: $T = 296$ K; $P = 100$ Torr; $[CH_3I] = 1.94 \times 10^{13}$ molecules cm^{-3} (□) and 1.34×10^{14} molecules cm^{-3} (+); $[Cl_2SO] = 2.07 \times 10^{13}$ molecules cm^{-3}; $[N_2]$ = balance; PRF = 5 Hz; $F_{(248nm)} = 2.34 \times 10^{15}$ photons cm^{-2}; $\lambda_{ex} = 360.57$ nm. Top panel: bimolecular plots of $(\lambda_+ + \lambda_-)$ against $[CH_3I]$ at 296 K. Experimental conditions: $T = 296$ K; $P = 100$ Torr; $[Cl_2SO] = 7.21 \times 10^{12}$ molecules cm^{-3}; $[N_2]$ = balance; PRF = 5 Hz; $F_{(248nm)} = 4.64 \times 10^{15}$ photons cm^{-2} (Δ) and 5.21×10^{16} photons cm^{-2} (O); $\lambda_{ex} = 360.57$ nm. From the linear fits: $m = -(1.03 \pm 0.15) \times 10^{-11}$ cm^3 molecule^{-1} s^{-1}, $c = -(2756 \pm 83)$ s^{-1} (Δ), and $m = -(2.61 \pm 0.59) \times 10^{-11}$ cm^3 molecule^{-1} s^{-1}, $c = -(3605 \pm 306)$ s^{-1} (O).

the $T \sim 200$ K data, pseudo-first-order formation and removal rates were obtained by fitting eq I to the experimental data:

$$\mathrm{LIF} = \frac{k_f'[Cl]_0}{(k_f' - k_r')}(\exp(-k_r' t) - \exp(-k_f' t)) + b \qquad \text{(I)}$$

where LIF is the fluorescence signal at a time, t, after the photolysis laser pulse; k_f' is the pseudo-first-order adduct formation rate; k_r' is the first-order adduct removal rate; $[Cl]_0$ relates to the initial concentration of chlorine atoms generated by the photolysis laser; and b is a term allowing for slight positive baseline deviations from the pre-excimer laser back-

ground. Note that in fitting eq I to the experimental data, it is assumed that adduct dissociation to reactants is negligible at ~200 K; that is, $k_{-a} = 0$ in reaction Scheme 1.

Pseudo-first-order formation rates, k_f' were measured as a function of methyl iodide concentration (under pseudo-first-order conditions $[CH_3I]_0 \gg [Cl]_0$), allowing the rate coefficient for the $CH_3I + Cl$ reaction, k_1, to be determined via a bimolecular plot of kf' against $[CH_3I]$. Figure 3 displays some bimolecular plots for the $CH_3I + Cl$ reaction recorded at ~200 K and as a function of total pressure in N_2. The intercepts are all of similar magnitude, and no systematic relationship to the experimental conditions is evident. The average intercept value was (229 ± 285) s^{-1}, where the error represents 2σ uncertainty. Thus, it can be concluded that diffusion of Cl atoms and their reaction with species other than CH_3I were of slight but negligible consequence. Table 1 lists all determinations of the bimolecular rate coefficient, k_1, at ~200 K along with pertinent experimental conditions and relevant results from other studies. Although the rate coefficients, k_1, reported in Table 1 are the sum of all reactive channels in the $CH_3I + Cl$ reaction (see reaction Scheme 1), the Arrhenius data of Ayhens et al.[31] imply that the bimolecular reaction pathway (producing HCl) is negligibly small at 200 K ($k_{bi} = 1.1 \times 10^{-13}$ cm^3 molecule^{-1} s^{-1}), and hence, all reactivity can effectively be assigned to the association rate coefficient, and $k_1 = k_a$.

From the data obtained, the formation of the fluorescing species is clearly pressure-dependent, and the good agreement with the 218 K results of Ayhens et al.[31] (see Table 1) primarily indicates that this species is a product of the $CH_3I + Cl$ reaction and almost certainly the CH_3I-Cl adduct. Pressure-dependent rate coefficients are often evaluated by a Troe formulation, such as eq II,

$$k_{([M],T)} = \frac{k_0 k_\infty [M] F_c^x}{(k_\infty + k_0[M])} \qquad \text{(II)}$$

where $X = \{1 + [\log (k_0[M]/k_\infty)]^2\}^{-1}$; k_∞ and k_0 are the high- and low-pressure rate coefficients, respectively; and F_c is the broadening coefficient. When eq II is fit to the experimental data, parameters of $k_\infty = 4.18 \pm 0.42 \times 10^{-11}$ cm^3 molecule^{-1} s^{-1}, $k_0 = 1.73 \pm 0.53 \times 10^{-29}$ cm^6 molecule^{-2} s^{-1}, and $F_c = 0.79 \pm 0.15$ are returned, in reasonable agreement with Ayhens et al.[31] ($k_\infty = 4.0 \times 10^{-11}$ cm^3 molecule^{-1} s^{-1}, $k_0 = 2.0 \times 10^{-29}$ cm^6 molecule^{-2}s^{-1}, $F_c = 0.63$). At higher pressures, the temperature of the reaction cell deviates above that of the coolant (195 K) due to inefficient thermalization of the N_2 bath gas.

The CH_3I-Cl removal rate, k_r', was dependent on both $[Cl_2SO]$ and $[CH_3I]$, as shown in Figure 4. The $[CH_3I]$ dependence on the rate of removal of CH_3I-Cl was observed to be independent of pressure, with an average effective bimolecular rate coefficient of $k = (6.9 \pm 1.9) \times 10^{-13}$ cm^3 molecule^{-1} s^{-1}. Bilde and Wallington[33] speculated that CH_3I-Cl may react with CH_3I with a rate coefficient of similar magnitude, although the CH_3Cl yield (postulated as a product of this reaction) observed in their work displayed a complex and nonlinear dependence on $[CH_3I]$, suggesting more than one route to its formation. In a very recent study of CH_3I-Cl,[34] the rate coefficient for its self-reaction at 250 K and 300 Torr N_2 was determined to be $k = (3.5 \pm 1.2) \times 10^{-10}$ cm^3 molecule^{-1} s^{-1}. If it is assumed, therefore, that the adduct reacts rapidly with radical species, the observed loss rate could be due to the reaction $CH_3 + CH_3I-Cl \rightarrow CH_3I + CH_3Cl$, giving a rate coefficient for this reaction of $k_4 = (3.0 \pm 0.9) \times 10^{-10}$ cm^3 molecule^{-1} s^{-1} if $[CH_3]$ is calculated from the extent of CH_3I photolysis at 248 nm. To check if such chemistry could explain the observed temporal profile of CH_3I-Cl in our experimental system, the kinetic traces displayed in Figure 4 were modeled using FACSIMILE[46] with the reaction scheme given in Table 2. Because LIF is not an absolute technique, this procedure first required converting the CH_3I-Cl LIF signal into a concentration. Initial concentrations of $[Cl]_0$, $[CH_3I]_0$, and $[CH_3]_0$ were entered into the model as defined by the experimental conditions and the absorption cross section and branching ratios for the photolysis of Cl_2SO[40] and CH_3I[41] at 248 nm. The model chemistry initially consisted of reactions 1−5 and 7 from Table 2, which also lists kinetic data for these reactions. The loss of Cl atoms (other than reaction with CH_3I), k_2, was obtained from the average intercept to the bimolecular plots of k_f' against $[CH_3I]$, and the diffusive loss rate of CH_3I-Cl, k_7, was estimated as 20 s^{-1}. The temporal profile of CH_3I-Cl was simulated over the experimental time range, and the experimental data were converted to units of concentration by normalization to the peak model concentration. The FACSIMILE model was then used to fit the normalized experimental data. Although the model fit to the experimental data was reasonable, some discrepancy was observed, and particularly with respect to the adduct decay. Additionally, the reaction of CH_3I-Cl with ClSO radicals (generated by the excimer laser photolysis of Cl_2SO) was therefore entered into the model, which was instructed to return a rate coefficient, k_6, for this process. The concentration of ClSO generated by the excimer laser, $[ClSO]_0$, was entered as an additional initial parameter, and the initial concentration of Cl atoms was floated in the model fitting to allow sufficient flexibility. The average rate coefficient returned by the model was $k_6 = (3.1 \pm 0.3) \times 10^{-10}$ cm^3 molecule^{-1} s^{-1}, where the error is the 2σ standard deviation of the three independent model determinations, and the initial Cl atom concentration returned by the model was always within 97% of the initial value entered. The model fits to the experimental traces are displayed in the bottom panel of Figure 4. The high precision to the model determination of k_6 indicates that this reaction is occurring in the experimental system. The magnitude of this rate coefficient is similar to that of the adduct self-reaction[34] and that of the hypothesized reaction of $CH_3I-Cl + CH_3$, and hence, CH_3I-Cl appears to react close to the gas kinetic limit with many radical species, presumably because the CH_3I component of the adduct can act as an intramolecular third body. Finally, the FACSIMILE model was used to generate pseudo-first-order formation and removal rates of CH_3I-Cl under the experimental conditions of the bimolecular experiment performed at 251 Torr and 216 K. Kinetic traces were simulated under the exact experimental conditions and incorporating reactions 1−7 in the FACSIMILE model (after adjusting any rate coefficients accordingly). Equation I was then fit to the model outputs returning values for kf' and kr', which are displayed in Figures 3 and 4, respectively.

TABLE 3: Experimental Conditions and Determinations of k_a, k_{-a}, and K_p for the reaction $CH_3I + Cl \leftrightarrow CH_3I-Cl$ at 296 K[a]

P	$[Cl_2SO]$	$\Delta[CH_3I]$	F	$-m$	$-c$	k_a	k_{-a}	K_p
21.5	3.10	439	24.5	12.6	37.7	3.75	16.3	55.6 ± 44.6
101.1	3.16	248	3.13	10.3	37.1	8.42	32.3	63.0 ± 36.4
101.6	0.72	7.26	4.64	10.3	27.6	7.98	24.3	79.2 ± 12.0
101.8	0.72	7.26	52.1	26.1	36.0	8.06	24.2	80.3 ± 19.5
100.4	2.06	11.5	2.55	10.8	24.7	9.11	24.8	88.8 ± 25.4
501.4	2.09	23.4	2.55	17.9	71.0	16.2	67.3	58.3 ± 14.8
101.0[a]	2.20	81.9	24.5	12.1	26.3	3.22	10.4	74.5 ± 29.5

[a] All experiments were conducted in N_2 with the exception of a, in which the bath gas was He. Units: P = Torr; [] = 10^{13} molecules cm^{-3}; $F_{(248nm)} = 10^{15}$ photons cm^{-2}; (m, k_a) = 10^{-12} cm^3 molecule^{-1} s^{-1}; (c, k_{-a}) = 10^2 s^{-1}; $K_p = 10^3$ atm^{-1}.

In conclusion, at low temperature, all the kinetic features observed can be explained by reaction Scheme 1 and by reactions of the CH_3I-Cl adduct with free radicals. The rate coefficients derived from the model are in agreement with the experimental determined values. There is no need to invoke the reaction of the adduct with CH_3I, as proposed by Bilde and Wallington,[33] which implies that the adduct is more reactive than the more energetic Cl atom.

At room temperature, the $CH_3I + Cl$ reaction is reversible, and the kinetic analysis is complicated by significant dissociation of the adduct back to reactants (k_{-a}) and the higher rate coefficient of the bimolecular reaction channel ($k_{bi(296\ K)} = 7.97 \times 10^{-13}$ cm^3 molecule^{-1} s^{-1} [31]) to form HCl. Consequently, the rates of adduct formation and removal are intrinsically coupled, and the data must be analyzed using the full analytical solution to reaction Scheme 1, given by eq III.

$$\mathrm{LIF} = \frac{k_a'[Cl]_0}{(\lambda_+ - \lambda_-)}(\exp(\lambda_+ t) - \exp(\lambda_- t)) + b \qquad \text{(III)}$$

where

$$\lambda_\pm = \frac{-(k_a' + k_{bi}' + k_2' + k_{-a}' + k_{loss}') \pm \sqrt{(k_a' + k_{bi}' + k_2' + k_{-a}' + k_{loss}')^2 - 4[(k_a' + k_{bi}' + k_2')(k_{-a}' + k_{loss}') - k_a' k_{-a}']}}{2} \qquad \text{(IV)}$$

Note that in eq IV, k_{loss}' corresponds to the sum of all pseudo-first-order adduct loss processes given in Table 2 (i.e., $k_3' + k_4' + k_6' + k_7'$). The assumption is again made that the concentrations of species reacting with the adduct are in excess of it so that pseudo-first-order loss can be approximated. At room temperature, k_6 is not a second-order process (although ClSO and Cl are generated by the excimer laser in equal yield), because adduct formation is reversible, and the concentration of CH_3I-Cl is thus always much lower than that of ClSO. Although reaction 3 is a second-order reaction, it is less important than the other adduct reactions and can be adequately approximated as a first-order process. From eq IV, it is clear that the sum of λ_+ and λ_- is equal to the sum of all pseudo-first-order rate coefficients in the system, and a plot of ($\lambda_+ + \lambda_-$) against [CH_3I] should yield a straight line with a slope equal to the sum of all pseudo-first-order processes that are dependent on the concentration of methyl iodide (i.e., to a first approximation: $ka' + kbi' + k4'$) and an intercept that is equal to the sum of all pseudo-first-order processes that are independent of [CH_3I] (i.e., to a first approximation: $k_{-a}' + k_2' + k_3' + k_6' + k_7'$). Figure 5 displays kinetic traces of CH_3I-Cl recorded at room temperature for different concentrations of CH_3I (the difference in adduct yield illustrating the reversible nature of adduct formation) and plots of ($\lambda_+ + \lambda_-$) against [CH_3I] for two bimolecular experiments conducted under identical conditions with the exception of excimer laser power.

From the bimolecular plots, it can clearly be seen that both intercept, c, and slope, m, significantly increase with increasing excimer laser fluence, providing further evidence that CH_3I-Cl reacts with itself and the photolysis products of CH_3I and Cl_2SO. To a first approximation, the difference in the slopes divided by the difference in percentage extent of photolysis (i.e., $F_{(248nm)}\sigma_{(248nm)}$) gives the bimolecular rate coefficient, $k_4 = (3.8 \pm 1.5) \times 10^{-10}$ cm^3 molecule^{-1} s^{-1}. This value is in good agreement with that predicted at ~200 K, which suggests that the adduct does not significantly react with CH_3I. As previously stated, adduct dissociation is sufficiently fast at 296 K (~2500 s^{-1} in 100 Torr N_2) that the concentration of ClSO is always in excess to that of CH_3I-Cl, and the difference in intercept values of the bimolecular plots can be attributed to reaction 6, to a first approximation. Dividing this difference, $\Delta c = (849 \pm 317)$ s^{-1}, by the difference in ClSO concentration (Δ[ClSO] $= 2.32 \times 10^{12}$ molecules cm^{-3}) gives a bimolecular rate coefficient, $k_6 = (3.7 \pm 1.4) \times 10^{-10}$ cm^3 molecule^{-1} s^{-1}, also in good agreement with that determined at ~200 K. Having obtained approximations for k_4 and k_6 at 296 K (and assuming that adduct self-reaction contributes negligibly to the overall reaction kinetics at room temperature), k_a and k_{-a} (and thus K_p) can be evaluated from the experimental data:

$$k_a = -(m - k_{bi} - k_4')$$

$$k_{-a} = -(c - k_6' - k_2' - k_7')$$

$$K_p = \frac{k_a}{k_{-a}RT} \qquad \text{(V)}$$

where k_{bi} is evaluated from the Arrhenius data of Ayhens et al.[31] ($k_{(296K)} = 7.97 \times 10^{-13}$ cm^3 molecule^{-1} s^{-1}); k_4' is the contribution from reaction 4 to the slope of a bimolecular plot (i.e., $k_4\sigma F$); k_6' is the contribution from reaction 6 to the intercept of a bimolecular plot (i.e., k_6[ClSO]); and k_2' and k_7' are assumed the values at ~200 K (i.e., 220 s^{-1} and 20 s^{-1}, respectively). Table 3 lists all values of k_a, k_{-a} and K_p at 296 K, determined by this procedure, along with the most pertinent experimental conditions. The average equilibrium constant obtained [$K_p = (70.9 \pm 27.4) \times 10^3$ atm^{-1}] is in excellent agreement with that calculated from the thermochemical data of Ayhens et al.[31] [$K_p = 72.6 \times 10^3$ atm^{-1}].

The CH_3I-Cl adduct was not observed to undergo significant reaction with molecular oxygen at ~200 or 296 K ($k < 10^{-16}$ cm^3 molecule^{-1} s^{-1}) upon addition of up to 2 Torr O_2 to the reagent mixture.

TABLE 4: Pressure-Dependent Bimolecular Rate Coefficient (k_8) Determinations for the $CH_2I_2 + Cl$ Reaction at $T \approx 200$ K[a,b]

T/K	P/Torr	$[Cl]_0$[a]	$[CH_2I_2]$[b]	$k_8/10^{-12}$ cm^3 molecule^{-1} s^{-1}
200.0	10.3	0.75	0−80.5	12.3 ± 4.2
200.2	20.1	0.83	0−98.7	21.0 ± 11.9
200.4	39.8	0.44	0−75.1	29.2 ± 4.6
201.9	69.5	0.45	0−73.6	30.9 ± 5.4
203.8	100.2	0.45	0−79.3	48.6 ± 10.7
216.2	248.3	0.42	0−75.3	57.6 ± 7.6
215.9	496.7	0.85	0−75.2	60.4 ± 21.9

[a] Estimated initial Cl atom concentration generated by 248 nm photolysis of Cl_2SO,/10^{12} molecules cm^{-3}. [b] Range of CH_2I_2 concentrations employed/10^{12} molecules cm^{-3}.

Laser-Induced Fluorescence Spectroscopy of the CH_3I-Cl Adduct. The LIF excitation spectrum of the CH_3I-Cl adduct was recorded between 345 and 375 nm at 296 and 204 K, as shown in Figure 6. There is little temperature dependence, and the broad spectra are indicative of a polyatomic species with many modes of internal motion, although there is some evidence of vibronic structure. Two regular features with frequencies of ~150 and 40 cm^{-1} were observed. Indeed, previous theoretical works [30,31]have calculated the two lowest vibrational frequencies of the CH_3I-Cl electronic ground state to be in the 90−170 cm^{-1} range. In the LIF spectra, a generic change in spectral structure is observed at a wavelength of ~365 nm (see Figure 6), possibly corresponding to the band origin of the electronic transition. To longer wavelengths, the spectral

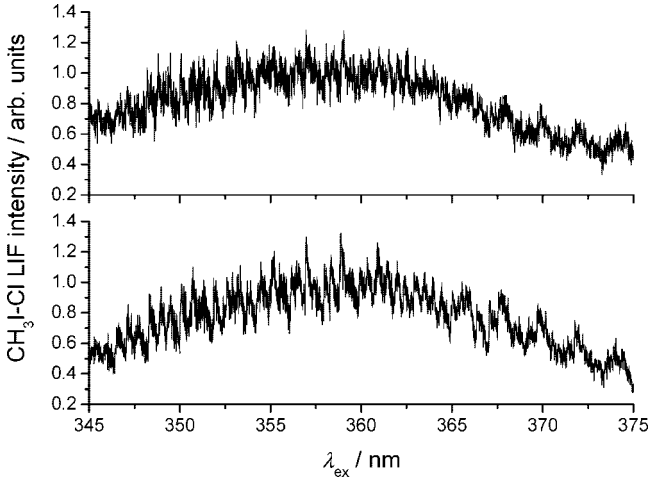

Figure 6. Laser excitation spectra of the CH_3I-Cl adduct at 296 K (top panel) and 204 K (bottom panel). Experimental conditions: P = 100 Torr; $[Cl_2SO] = 6.3 \times 10^{13}$ molecules cm^{-3}; $[CH_3I] = 4.3 \times 10^{14}$ molecules cm^{-3}; $[N_2]$ = balance; PRF = 10 Hz; $\Delta t = 150$ μs; $F_{(248nm)} = 5.21 \times 10^{16}$ photons cm^{-2}.

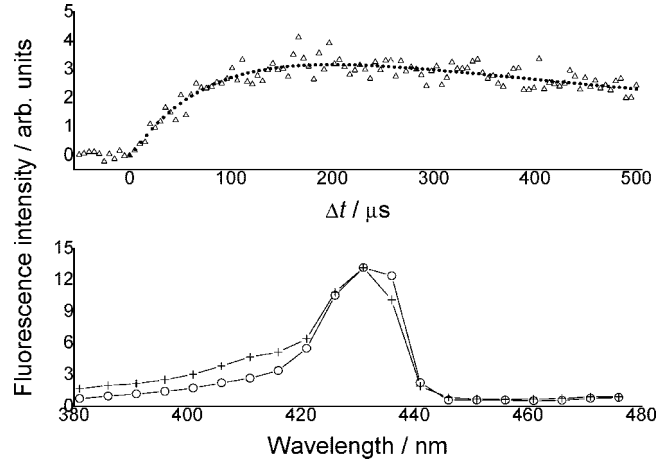

Figure 7. Bottom panel: dispersed fluorescence spectra of the CH_3I-Cl adduct at 296 K and 30 Torr (+) and 300 Torr (o). Experimental conditions: $[Cl_2SO] = 6.0 \times 10^{13}$ molecules cm^{-3}; $[CH_3I] = 2.3 \times 10^{15}$ molecules cm^{-3}; $[N_2]$ = balance; $\Delta t = 40$ μs; PRF = 10 Hz; $F_{(248nm)} = 3.3 \times 10^{16}$ photons cm^{-2}; $\lambda_{ex} = 365.57$ nm; monochromator resolution = 5 nm fwhm. Note that the data have been normalized so that the peak fluorescence signals of the spectra are equal at ~430 nm. The fluorescence signal is relative to zero; that is, fluorescence is occurring at all wavelengths. Top panel: CH_3I-Cl kinetic trace recorded by monitoring adduct fluorescence at ~430 nm through the monochromator at 5 nm fwhm resolution. Experimental conditions: $T = 296$ K; $P = 20.2$ Torr; $[Cl_2SO] = 2.6 \times 10^{13}$ molecules cm^{-3}; $[CH_3I] = 5.3 \times 10^{14}$ molecules cm^{-3}; $[N_2]$ = balance; PRF = 5 Hz; $F_{(248nm)} = 3.3 \times 10^{16}$ photons cm^{-2}; $\lambda_{ex} = 365.57$ nm. The dotted line (·) is a fit of eq III to the experimental data. From the fit, $(\lambda_+ + \lambda_-)_{exp} = -(13620 \pm 2154)$ s^{-1}. From the experimental conditions and employing the rate coefficients previously determined, $(\lambda_+ + \lambda_-)_{calc} = -12120$ s^{-1}.

features become more widely spaced, potentially due to hotband excitation from the adduct ground state, and at wavelengths below ~365 nm, the spectral structure becomes more crowded, possibly due to the population of highly excited vibrational states in the electronically excited state of CH_3I-Cl. Enami et al.[27] speculated that the adduct absorption observed in their work at visible wavelengths, between 405 and 532 nm, was due to the red end of an electronic transition originating at either 337 or 307 nm (these band origins were theoretically derived). However, this excitation scheme can be discounted for two reasons: First, a 532 nm transition between two states with an energy separation of 337 nm requires ~10 900 cm^{-1} of ground-state excitation, where an infinitesimal Boltzmann population would be present. Second, even if the population distribution within the adduct ground state were nonthermal, ~10 900 cm^{-1} (~130 kJ mol^{-1}) of internal excitation is more than twice the experimentally determined binding enthalpy of the CH_3I-Cl ground state.[31] These arguments become even more severe if a 307 nm band origin is considered.

To further probe the spectroscopy of the CH_3I-Cl adduct, the dispersed fluorescence spectrum was recorded using a monochromator in 5 nm intervals at 5 nm resolution, following laser excitation at 365 nm. The spectrum was found to be pressure-dependent (see Figure 7), with a smaller fluorescence intensity at lower wavelengths at higher pressures, indicative of fluorescence being preceded by collision-induced vibrational energy transfer (VET) in the adduct excited state. No fluorescence was observed blue-shifted relative to the excitation wavelength, indicating that the adduct ground state was rapidly thermalized under the experimental conditions, and only very weak fluorescence was observed beyond 445 nm. If it is assumed that 365 nm corresponds to the band origin of the electronic transition (as discussed above) and that the cutoff wavelength of fluorescence (~445 nm) corresponds to the difference in energy between the ground vibrational level of the electronically excited adduct state (populated by VET) and the dissociation limit of the ground electronic state, the CH_3I-Cl bond strength can be estimated as ~59 kJ mol^{-1}, which is in reasonably good agreement with the experimentally determined value [(52 ± 3) kJ mol^{-1}].[31] The dispersed fluorescence spectrum was unambiguously assigned to CH_3I-Cl by recording a kinetic trace through the monochromator, at a wavelength of 430 nm, in which the temporal evolution of CH_3I-Cl was in excellent agreement with the experimental conditions and the reaction kinetics previously determined. Finally, a dispersed fluorescence spectrum was recorded at 300 Torr for a 350 nm excitation wavelength. No discernible difference from the 300 Torr spectrum recorded after 365 nm adduct excitation was apparent.

The fluorescence lifetime of the adduct could not be accurately determined (because the fluorescence did not sufficiently extend the duration of the excitation laser pulse), although it is estimated that fluorescence quenching of the excited electronic state of CH_3I-Cl by N_2 at 296 K occurs with a rate coefficient on the order of 5×10^{-12} cm^3 $molecule^{-1}$ s^{-1}, and the zero-pressure fluorescence lifetime is on the order of 25 − 30 ns, possibly indicating the influence of predissociation in the excited electronic state.

Kinetics of the CH_2I_2 + Cl Reaction and of the ICH_2I-Cl Adduct. There has been only one very recent previous kinetic study of the CH_2I_2 + Cl reaction, performed at very low pressure (<3 mTorr) in a Knudsen cell.[47] No pressure dependence was performed to determine falloff parameters for formation of the adduct. In this work, we sought kinetic information via LIF detection of the ICH_2I-Cl adduct. Initially, the kinetics of the CH_2I_2 + Cl reaction were investigated at ~200 K by measuring the pseudo-first-order formation rate of ICH_2I-Cl in Cl_2SO/CH_2I_2/N_2/248 nm reagent mixtures, using excess CH_2I_2, as a function of total pressure. At, $T \approx 200$ K, it was assumed that the CH_2I_2 + Cl reaction mechanism is analogous to that of CH_3I + Cl, and all kinetic traces were analyzed using eq I. Figure 8 displays a kinetic trace of the ICH_2I-Cl adduct and bimolecular plots as a function of pressure, and Table 4 lists all bimolecular rate coefficients, k_8, determined and the pertinent experimental conditions under which they were obtained.

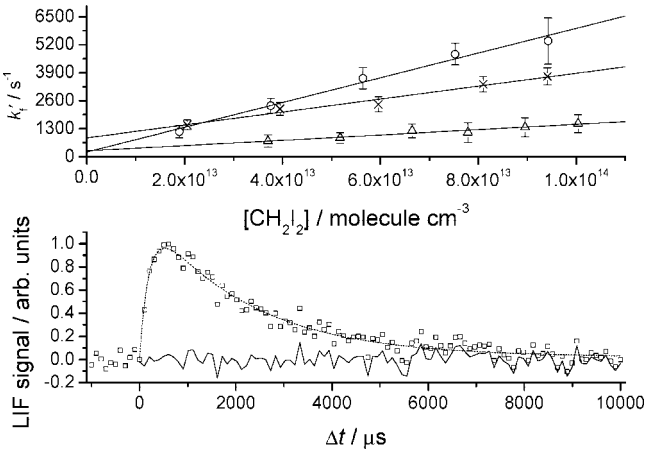

Figure 8. Bottom panel: Temporal profile of ICH_2I-Cl fluorescence signal in a $Cl_2SO/CH_2I_2/N_2/248$ nm photolysis mixture. Fit of eq I (▪▪▪) to the experimental data (□). Experimental conditions: $T = 204$ K; $P = 100$ Torr; $[Cl_2SO] = 1.56 \times 10^{13}$ molecules cm^{-3}; $[CH_2I_2] = 7.90 \times 10^{13}$ molecules cm^{-3}; $[N_2]$ = balance; PRF = 5 Hz; $F_{(248nm)} = 4.2 \times 10^{15}$ photons cm^{-2}; $\lambda_{ex} = 365.57$ nm. Top panel: pressure-dependent bimolecular plots for the $CH_2I_2 + Cl$ reaction at ~200 K. $P = 10.3$ Torr (Δ), 69.5 Torr (×), and 248.3 Torr (O). Other experimental conditions are given in Table 4.

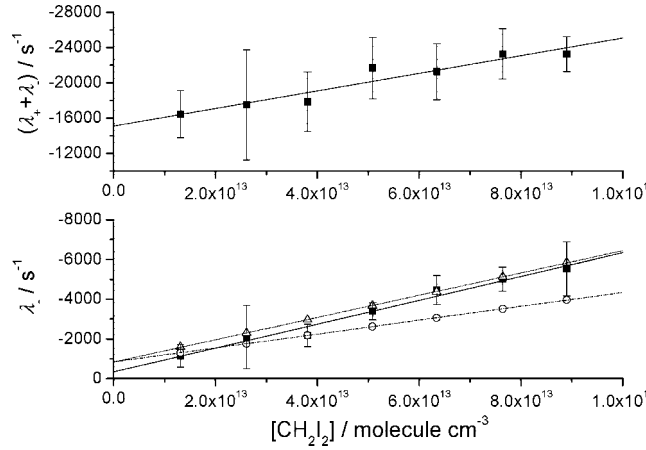

Figure 9. Top panel: bimolecular plot of $(\lambda_+ + \lambda_-)$ against $[CH_2I_2]$ for the $CH_2I_2 + Cl$ reaction. Experimental conditions: $T = 296$ K; $P = 100$ Torr (N_2); $[Cl_2SO] = 1.05 \times 10^{13}$ molecules cm^{-3}; $[N_2]$ = balance; PRF = 5 Hz; $F_{(248nm)} = 4.27 \times 10^{16}$ photons cm^{-2}; $\lambda_{ex} = 365.57$ nm. From the linear fit: $c = -(15\,100 \pm 2000)$ s^{-1}; $-m = -(10.0 \pm 3.6) \times 10^{-11}$ cm^3 molecule^{-1} s^{-1}. Bottom panel: plot of λ_- against $[CH_2I_2]$ (■), along with model calculations (see text for details), assuming that ICH_2I-Cl dissociation produces either reactants (O) or products (Δ).

TABLE 5: Reaction Enthalpies (kJ mol^{-1}) for the Formation of HCl/ICl/I Atoms from the Reaction of Relevant Alkyliodides with Atomic Chlorine at 298 K[a]

iodoalkane	$\Delta H^0_{r,298}$(HCl)	$\Delta H^0_{r,298}$(ICl)	$\Delta H^0_{r,298}$(I)
CH_3I	2.3	28.4	−110.7
CH_2ICl	−8.7	6.4	−117.0
CH_2I_2	2.4	8.3	−125.4

[a] The reaction enthalpies are calculated from the known standard enthalpies of formation of the various products and reactants,[43] with the exceptions of CHICl and CHI_2, which are obtained from the literature.[36,44]

As for the $CH_3I + Cl$ reaction, the rate coefficient is pressure-dependent at ~200 K. Fitting the experimental data to eq II yields the pressure-dependent Troe parameters: $k_0 = (5.2 \pm 1.1) \times 10^{-29}$ cm^6 molecule^{-2} s^{-1}; $k_\infty = (7.1 \pm 1.2) \times 10^{-11}$ cm^3 molecule^{-1} s^{-1}; and $F_c = 0.79$ (the latter was fixed to the value obtained for the $CH_3I + Cl$ reaction). Also in agreement with the CH_3I-Cl kinetic study, the pseudo-first-order loss rate, k_r', of ICH_2I-Cl was found to be dependent on the concentration of CH_2I_2, with an average effective bimolecular rate coefficient of $k = (3.1 \pm 2.4) \times 10^{-12}$ cm^3 molecule^{-1} s^{-1}. If it is assumed that loss is due to the reaction of ICH_2I-Cl with CH_2I radicals (or I atoms) generated by the 248 nm excimer laser photolysis of CH_2I_2, an average bimolecular rate coefficient (i.e., from all bimolecular experiments) of $k = (4.9 \pm 3.9) \times 10^{-10}$ cm^3 molecule^{-1} s^{-1} is obtained, which is in good agreement with that hypothesized for the reaction of CH_3I-Cl with CH_3 radicals. In accordance with the reaction kinetics of CH_3I-Cl, no significant reaction of ICH_2I-Cl with O_2 was observed.

The data are wholly consistent with adduct formation from the reaction of Cl with CH_2I_2, with the adduct being significantly stabilized at low temperature. A similar finding has already been discussed above for the adduct formed in the $CH_3I + Cl$ reaction. However, both of these results are different from those obtained for the $CH_2ICl + Cl$ reaction, for which only a weak pressure dependence was observed.[35] Table 5 lists the 298 K enthalpy change for the reactions of CH_3I, CH_2ICl, and CH_2I_2 with atomic chlorine, in which a number of different reaction mechanisms are considered (i.e., H atom abstraction, forming HCl; I atom abstraction, forming ICl; or halogen atom substitution, forming I atoms). In all cases, halogen atom substitution is most exothermic. However, I atoms have not been observed as reaction products in the reaction of either CH_3I or CH_2ICl with Cl atoms, presumably because these mechanisms are entropically hindered. On this basis, we suggest that this channel is not occurring.

Whereas HCl is known to be the major product of the reaction of $CH_3I + Cl$,[22,29] ICl is formed in unity yield from the reaction of chloroiodomethane with Cl,[35,36] and given the thermochemical data in Table 5, ICl may also therefore be expected to be the predominant product of the $CH_2I_2 + Cl$ reaction. Indeed, at low pressures (<3 mTorr) in a Knudsen cell, the yield of HCl from this reaction was determined to be 55 ± 10%,[47] and given that the CH_2I_2-Cl adduct is not stabilized under these conditions, this implies a significant yield of ICl formed via an additional dissociation channel of the adduct.

To further investigate the mechanism of $CH_2I_2 + Cl$ reaction, a series of k' values was measured to determine a bimolecular rate coefficient at room temperature and 100 Torr total pressure N_2. Kinetic traces were analyzed with eq III. Figure 9 displays the resultant plot of $(\lambda_+ + \lambda_-)$ against $[CH_2I_2]$ using the complete solution for reaction Scheme 2, with $(\lambda_+ + \lambda_-)$ being equal to the sum of all the removal processes in the system. From the large intercept of the bimolecular plot, it can be seen that significant adduct dissociation must occur (cf. Figure 5), although the identity, that is, k_{-a} or k_p, of the dissociation products is unclear. If adduct dissociation exclusively regenerates $CH_2I_2 + Cl$ (in a fashion analogous to the $CH_3I + Cl$ reaction), then the experimental kinetic traces must be strictly analyzed using eq III (because adduct formation and removal are intrinsically coupled). However, if adduct dissociation produces exclusively other products (as in the $CH_2ICl + Cl$ reaction), then ICH_2I-Cl formation and removal will be uncoupled, and the experimental data can be adequately analyzed using eq I. To investigate this question, kinetic traces of ICH_2I-Cl were simulated under the conditions of the bimolecular experiment using the FACSIMILE model previously outlined. In the model, a rate coefficient that is analogous to k_4 was assigned a value of 4.9×10^{-10} cm^3 molecule^{-1} s^{-1}

(in accordance with the $T \approx 200$ K investigation), and it was assumed that the ICH_2I-Cl adduct both self-reacts and reacts with ClSO radicals at the same rates as with CH_3I-Cl. Reaction 5 was altered to the self-reaction of CH_2I radicals[45] and assigned a value of $k = 4 \times 10^{-11}$ cm^3 molecule^{-1} s^{-1}. The pseudo-first-order loss of Cl atoms, k_2, was assigned a value of 740 s^{-1} (the average intercept to the bimolecular plots generated in the $T \approx 200$ K experiments). The reaction of CH_2I_2 with Cl atoms ($k_8 = k_a + k_{bi}$) was assigned a value of $k_8 = 6.7 \times 10^{-11}$ cm^3 molecule^{-1} s^{-1} (corresponding to the slope of the bimolecular plot in Figure 9, once corrected for reaction of the adduct with CH_2I radicals, and ignoring any contribution from the self-reaction of ICH_2I-Cl). k_{bi} was assigned the same value as k_{1b}, the bimolecular rate constant for HCl formation from $Cl+CH_3I$.

Preliminary results on the HCl yield from this reaction using an infrared diode laser experiment in Leeds[48] indicate the HCl yield is less than 10% at 20 Torr total pressure, which implies in our simulations that we are underestimating this channel. However, the simulations are designed to quantify the rate of adduct loss rather than the yield of the adduct in this reaction. ICH_2I-Cl dissociation was assigned a unimolecular rate coefficient of 13 200 s^{-1} (at 296 K and 100 Torr N_2) after correcting the intercept of the bimolecular plot in Figure 9 for k_2 and k_6 (and ignoring the contribution from adduct self-reaction). Kinetic traces were simulated for either dissociation channel (−9a) or (9p) (see Table 2), and eq III was fit to the model output generating a series of values for λ_+ and λ_-. Modeled and experimental values of λ_- are plotted against $[CH_2I_2]$ in the bottom panel of Figure 9. From this Figure, it appears that dissociation via k_{9p} to other products provides a better description of the data than k_{9r}. This approximate analysis is designed to demonstrate the occurrence of this additional adduct loss, but an equally good description to the data in Figure 9 derives from both k_{9p} and k_{9r} operating, where $k_{9p} > k_{-9a}$. The spectrum of the CH_3I-Cl adduct is similar to that of ICH_2I-Cl (see below), and hence, it is reasonable to expect the binding energies also to be similar. Such an assumption is supported by ab initio calculations presented in Stefanopoulos et al., who calculate a binding energy for the ICH_2I-Cl adduct of 51.9 kJ mol^{-1}. On the basis of the value of k_{-a} for CH_3ICl given in Table 4, a reasonable estimate of k_{-9a} for ICH_2I-Cl at 100 Torr total pressure is ∼3000 s^{-1}. If this value is used for k_{-9a}, then k_{9p} is equal to 10 200 s^{-1} (13 200−3000), which is consistent with $k_{9p} > k_{9r}$ and, hence, provides a reasonable description for λ_- in Figure 9. To rigorously analyze the data, a complete solution to reaction Scheme 2 ought to be used, but such a solution has too many parameters to uniquely identify the rate constants of the system with any confidence.

In conclusion, when comparing the two reactions $CH_3I + Cl$ and $CH_2I_2 + Cl$, the latter has an additional adduct dissociation channel to ICl, as is the case for $CH_2ClI + Cl$[36]. This additional channel for $CH_2I_2 + Cl$ results in a less than unity yield of HCl in the reaction, unlike the case for the $CH_3I + Cl$ reaction. This conclusion is supported both by preliminary experiments using an IR diode laser,[48] which indicate an HCl yield of <10% for $CH_2I_2 + Cl$ at 296 K and 20 Torr total pressure (He), and by the Knudsen cell[47] experiment at low pressure (<3 mTorr), for which the yield of HCl was found to be 55 ± 10%. Despite the very low pressure, the HCl yield in the Knudsen experiment is not unity, suggesting a significant yield of ICl, originating from a short-lived adduct with considerable internal energy. Reaction Scheme 2 should therefore be thought of as a chemical activation scheme, containing both internally excited and thermalized (after collisions) CH_2I_2-Cl adducts.

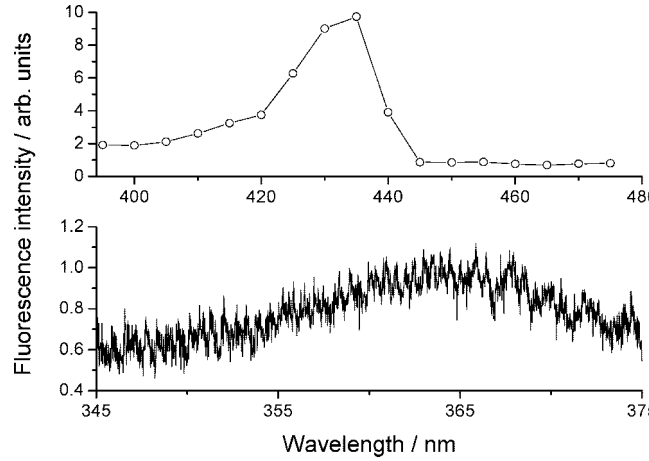

Figure 10. Bottom panel: LIF excitation spectrum of the ICH_2I-Cl adduct at 296 K. Experimental conditions: $P = 100$ Torr; $[Cl_2SO] = 2.1 \times 10^{13}$ molecules cm^{-3}; $[CH_2I_2] = 4.2 \times 10^{13}$ molecules cm^{-3}; $[N_2]$ = balance; PRF = 10 Hz; $\Delta t = 150$ μs; $F_{(248nm)} = 7.61 \times 10^{16}$ photons cm^{-2}. Top panel: dispersed fluorescence spectrum of the ICH_2I-Cl adduct in 100 Torr N_2. Experimental conditions: $T = 296$ K; $[Cl_2SO] = 3.2 \times 10^{13}$ molecules cm^{-3}; $[CH_2I_2] = 4.2 \times 10^{13}$ molecules cm^{-3}; $[N_2]$ = balance; PRF = 10 Hz; $\Delta t = 100$ μs; $F_{(248nm)} = 7.6 \times 10^{16}$ photons cm^{-2}; $\lambda_{ex} = 365.57$ nm. Note that both spectra are corrected for the probe laser background and are relative to an instrumental signal, in the absence of fluorescence, of zero.

Laser-Induced Spectroscopy of the ICH_2I-Cl Adduct. Figure 10 displays the LIF excitation spectrum of the ICH_2I-Cl adduct recorded over a 345−375 nm excitation wavelength range and the dispersed fluorescence spectrum of ICH_2I-Cl after excitation at 365 nm. The spectra are very similar in structure to those of the CH_3I-Cl adduct (Figures 67), but slightly red-shifted (<5 nm). The results suggest that the electronic structure of both adducts is very similar, in agreement with theoretical calculations on a number of RI-Cl adducts[27,28,30,36] and, likewise, the binding energies, assuming that the excitation-fluorescence scheme previously hypothesized for CH_3I-Cl is correct. Fluorescence quenching of the ICH_2I-Cl adduct by N_2 at 296 K proceeded with an estimated rate coefficient of $k \approx 1 \times 10^{-11}$ cm^3 molecule^{-1} s^{-1}, and the zero pressure fluorescence lifetime was on the order of 25−30 ns.

Future theoretical and experimental work is required to further elucidate the electronic structure of the CH_3I-Cl and ICH_2I-Cl adducts and the spectroscopic transitions responsible for the fluorescence observed in this work.

Conclusions

This work reports the detection of the CH_3I-Cl and ICH_2I-Cl adducts by LIF for the first time. Both species exhibit continuous fluorescence over an excitation wavelength range of 345−375 nm. Structural features in the LIF excitation spectra are identified with vibrational frequencies of 40 and 150 cm^{-1}. We speculate that the band origin of the electronic transition responsible for adduct fluorescence occurs at ∼365 nm. The dispersed fluorescence spectra indicate that fluorescence is predominantly red-shifted from the excitation wavelength, with a peak intensity in the 430−435 nm range, and that fluorescence intensity shifts to longer wavelengths with increasing pressure, indicative of the influence of VET in the adduct excited state. Only very weak fluorescence is observed at wavelengths greater than ∼445 nm, which we expect to correspond to the energy separation between the ground vibrational level of the electronically excited adduct state (populated by VET) and the dissocia-

tion limit of the adduct electronic ground state. Taking the hypothesized band origin of the electronic transition (365 nm), an adduct binding energy of ~59 kJ mol^{-1} is derived, which is in reasonable agreement with the preceding literature. Collisional quenching of adduct fluorescence by N_2 at 296 K was rapid ($k \approx (5-10) \times 10^{-12}$ cm^3 $molecule^{-1}$ s^{-1}), and the short fluorescence lifetime at zero pressure ($\tau \approx 25-30$ ns) may indicate the influence of predissociation in the electronically excited adduct state. Further theoretical and experimental work is required to probe the electronic structure and spectroscopic transitions of the CH_3I-Cl and ICH_2I-Cl adducts.

LIF of the CH_3I-Cl adduct was used to determine the reaction kinetics of the $CH_3I + Cl$ reaction. The results obtained are in reasonable agreement with the previous literature and strongly support the mechanism of the reaction first proposed by Ayhens et al.[31] At ~200 K, the reaction proceeds predominantly via irreversible adduct formation, and CH_3I-Cl removal is principally governed by reaction with radicals (CH_3 and ClSO) and adduct self-reaction, which proceed at rates near to the gas kinetic limit. At room temperature, the reaction of $CH_3I + Cl$ proceeds via reversible adduct formation, and adduct−radical reactions are also important. It would appear that the CH_3I component of the adduct acts as an intramolecular "third body", providing many modes of internal motion in which energy from radical−radical reactions can be dissipated.

The reaction kinetics of the $CH_2I_2 + Cl$ reaction has been investigated by LIF detection of the ICH_2I-Cl adduct. At ~200 K, the reaction kinetics are pressure-dependent, and the high pressure limit is reached at lower pressures than for the $CH_3I + Cl$ reaction. At room temperature and 100 Torr total pressure N_2, adduct dissociation is rapid (~14 000 s^{-1}), and it is speculated that this is primarily due to an additional product channel producing ICl.

Acknowledgment. We are grateful to the University of Leeds for the provision of a University Research Scholarship (T.J.G.).

References and Notes

(1) Notario, A.; Le Bras, G.; Mellouki, A. *J. Phys. Chem. A* **1998**, *102*, 3112–3117.
(2) Canosa-Mas, C. E.; Cotter, E. S. N.; Duffy, J.; Thompson, K. C.; Wayne, R. P. *Phys. Chem. Chem. Phys.* **2001**, *3*, 3075–3084.
(3) Wang, W.; Ezell, M. J.; Ezell, A. A.; Soskin, G.; Finlayson-Pitts, B. J. *Phys. Chem. Chem. Phys.* **2002**, *4*, 1824–1831.
(4) Thiault, G.; Mellouki, A.; Le Bras, G. *Phys. Chem. Chem. Phys.* **2002**, *4*, 2194–2199.
(5) Ezell, M. J.; Wang, W.; Ezell, A. A.; Soskin, G.; Finlayson-Pitts, B. J. *Phys. Chem. Chem. Phys.* **2002**, *4*, 5813–5820.
(6) Albaladejo, J.; Notario, A.; Cuevas, C. A.; Jiménez, E.; Cabañas, B.; Martinez, E. *Atmos. Environ.* **2003**, *37*, 455–463.
(7) Cuevas, C. A.; Notario, A.; Martinez, E.; Albaladejo, J. *Phys. Chem. Chem. Phys.* **2004**, *6*, 2230–2236.
(8) Cuevas, C. A.; Notario, A.; Martinez, E.; Albaladejo, J. *Atmos. Environ.* **2005**, *39*, 5091–5099.
(9) Keene, W. C.; Pszenny, A. A. P.; Jacob, D. J.; Duce, R. A.; Galloway, J. N.; Schultz-Tokos, J. J.; Sievering, H.; Boatman, J. F. *Global Biogeochem. Cycles* **1990**, *4*, 407–430.
(10) Singh, H. B.; Thakur, A. N.; Chen, Y. E.; Kanakidou, M. *Geophys. Res. Lett.* **1996**, *23*, 1529–1532.
(11) Keene, W. C.; Maben, J. R.; Pszenny, A. A. P.; Galloway, J. N. *Environ. Sci. Technol.* **1993**, *27*, 866–874.
(12) Spicer, C. W.; Chapman, E. G.; Finlayson-Pitts, B. J.; Plasteridge, R. A.; Hubbe, J. M.; Fast, J. D.; Berkowitz, C. M. *Nature* **1998**, *394*, 353–356.
(13) Tanaka, P. L.; Oldfield, S.; Neece, J. D.; Mullins, C. B.; Allen, D. T. *Environ. Sci. Technol.* **2000**, *34*, 4470–4473.
(14) Chang, S.; Allen, D. T. *Environ. Sci. Technol.* **2006**, *40*, 251–262.
(15) Ariya, P. A.; Niki, H.; Harris, G. W.; Anlauf, K. G.; Worthy, D. E. *Atmos. Environ.* **1999**, *33*, 931–938.
(16) Platt, U.; Allan, W.; Lowe, D. *Atmos. Chem. Phys.* **2004**, *4*, 2393–2399.
(17) Allan, W.; Lowe, D. C.; Gomez, A. J.; Struthers, H.; Brailsford, G. W. *J. Geophys. Res.* **2005**, *110* (D11), D11306/1−D11306/8.
(18) Lary, D. J. *Atmos. Chem. Phys.* **2005**, *5*, 227–237.
(19) Pechtl, S.; Lovejoy, E. R.; Burkholder, J. B.; von Glasow, R. *Atmos. Chem. Phys.* **2006**, *6*, 505–523.
(20) Saiz-Lopez, A.; Plane, J. M. C.; McFiggans, G.; Williams, P. I.; Ball, S. M.; Bitter, M.; Jones, R. L.; Hongwei, C.; Hoffman, T. *Atmos. Chem. Phys.* **2006**, *6*, 883–895.
(21) Saunders, R. W.; Plane, J. M. C. *Environ. Chem.* **2005**, *2*, 299–303.
(22) Plane, J. M. C.; Joseph, D. M.; Allan, B. J.; Ashworth, S. H.; Francisco, J. S. *J. Phys. Chem. A* **2006**, *110*, 93–100.
(23) Carpenter, L. J.; Sturges, W. T.; Penkett, S. A.; Liss, P. S.; Alicke, B.; Hebestreit, K.; Platt, U. *J. Geophys. Res.* **1999**, *104*, 1679–1689.
(24) Cotter, E. S. N.; Booth, N. J.; Canosa-Mas, C. E.; Gray, D. J.; Shallcross, D. E.; Wayne, R. P. *Phys. Chem. Chem. Phys.* **2001**, *3*, 402–408.
(25) Urbanski, S. P.; Wine, P. H. *J. Phys. Chem. A* **1999**, *103*, 10935–10944.
(26) (a) Dookwah-Roberts, V.; Soller, R.; Nicovich, J. M.; Wine, P. H. *J. Photochem. Photobiol. A* **2005**, *176*, 114–123. (b) Kleissas, K. M.; Nicovich, J. M.; Wine, P. H. *J. Photochem. Photobiol. A* **2007**, *187*, 1–9.
(27) Enami, S.; Hashimoto, S.; Kawasaki, M.; Nakano, Y.; Ishiwata, T.; Tonokura, K.; Wallington, T. J. *J. Phys. Chem. A* **2005**, *109*, 1587–1593.
(28) Enami, S.; Yamanaka, T.; Hashimoto, S.; Kawasaki, M.; Tonokura, K. *J. Phys. Chem. A* **2005**, *109*, 6066–6070.
(29) Kambanis, K. G.; Lazarou, Y. G.; Papagiannakopoulos, P. *Chem. Phys. Lett.* **1997**, *268*, 498–504.
(30) Lazarou, Y. G.; Kambanis, K. G.; Papagiannakopoulos, P. *Chem. Phys. Lett.* **1997**, *271*, 280–286.
(31) Ayhens, Y. V.; Nicovich, J. M.; McKee, M. L.; Wine, P. H. *J. Phys. Chem. A* **1997**, *101*, 9382–9390.
(32) Goliff, W. S.; Rowland, F. S. *Geophys. Res. Lett.* **1997**, *24*, 3029–3032.
(33) Bilde, M.; Wallington, T. J. *J. Phys. Chem. A* **1998**, *102*, 1550–1555.
(34) Dookwah-Roberts, V.; Nicovich J. M.; Wine, P. H. J. *Phys. Chem. A*, in press.
(35) Bilde, M.; Sehested, J.; Nielsen, O. J.; Wallington, T. J.; Meagher, R. J.; McIntosh, M. E.; Piety, C. A.; Nicovich, J. M.; Wine, P. H. *J. Phys. Chem. A* **1997**, *101*, 8035–8041.
(36) Kambanis, K. G.; Argyris, D. Y.; Lazarou, Y. G.; Papagiannakopoulos, P. *J. Phys. Chem. A* **1999**, *103*, 3210–3215.
(37) Qi, J.-X.; Wang, G.-J.; Han, K.-L.; Sha, Y.-X.; He, G.-Z.; Lou, N.-Q. *Mol. Phys.* **1997**, *92*, 71–75.
(38) Hoffmann, S. M. A.; Smith, D. J.; González, A.; Steele, T. A.; Grice, R. *Mol. Phys.* **1984**, *53*, 1067–1079.
(39) Gravestock, T. J. A kinetic and spectroscopic study of chemistry relating to the atmospheric role of iodine species. PhD Thesis, University of Leeds, September 2006.
(40) Baum, G.; Effenhauser, C. S.; Felder, P.; Huber, J. R. *J. Phys. Chem.* **1992**, *96*, 756.
(41) Sander, S. P.; Friedl, R. R.; Ravishankara, A. R.; Golden, D. M.; Kolb, C. E.; Kurylo, M. J.; Huie, R. E.; Orkin, V. L.; Molina, M. J.; Moortgat, G. K.; Finlayson-Pitts, B. J. *"Chemical Kinetics and Photochemical Data for Use in Atmospheric Studies: Evaluation Number 14"*, JPL Publication 02-25, February 1, 2003.
(42) NIST Chemical Kinetics Database: http://kinetics.nist.gov/kinetics/index.jsp.
(43) Atkinson, R.; Baulch, D. P.; Cox, R. A.; Crowley, J. N.; Hampson, R. F.; Hynes, R. G.; Jenkin, M. E.; Rossi, M. J.; Troe, J. *Atmos. Chem. Phys.* **2004**, *4*, 1461–1738.
(44) McMillen, D. F.; Golden, D. M. *Annu. Rev. Phys. Chem.* **1982**, *33*, 493–532.
(45) Sehested, J.; Ellermann, T.; Nielsen, O. J. *Int. J. Chem. Kinet.* **1994**, *26*, 259–272.
(46) Curtis, A. R.; Sweetenham, W. P. *FACSIMILE, AERE Harwell publication R 12805, Computer Science and Systems Division*; Harwell Laboratory: Oxfordshire, UK, 1987.
(47) Stefanopoulos, V. G.; Papadimitriou, V. C.; Lazarou, Y. G.; Papagiannakopoulos, P. *J. Phys. Chem. A* **2008**, *112*, 1526–1535.
(48) Seakins, P. W. University of Leeds, personal communication.

JP800372C